Received: 16 June 2021 | Accepted: 5 September 2021

DOI: 10.1002/pamm.202100090

Multi-layered tissue models in patient-specific simulations of aortic dissection

Richard Schussnig[1,2,*], **Kathrin Bäumler**[3], and **Thomas-Peter Fries**[1,2]

[1] Institute of Structural Analysis, Graz University of Technology, Lessingstraße 25/II, 8010 Graz, Austria
[2] Graz Center of Computational Engineering, Graz University of Technology, Krenngasse 37/I, 8010 Graz, Austria
[3] 3D and Quantitative Imaging Laboratory, Department of Radiology, Stanford University, Stanford, CA 94305, USA

In aortic dissections blood flows not only in the regular, true lumen but also between separated lamellae within the media of the aortic wall, in the so-called false lumen. Both lumina are separated by a dissection membrane, which may move substantially during the cardiac cycle, linking blood flow and vessel deformation. We employ strongly coupled fluid-structure interaction simulations incorporating an anisotropic, fiber-reinforced, hyperelastic continuum including layer-specific tissue parameters.

1 Introduction

In aortic dissection (AD), structurally impaired medial layers of the aortic wall are torn apart, creating a so-called *false lumen* in which blood flows parallel to the original *true lumen*. The thin and initially very flexible dissection membrane (or *flap*) heavily impacts blood flow which in turn governs flap motion. Corresponding hemodynamic quantities such as the pressure differential between true and false lumen (which is affected by flap motion) are related to false lumen growth and thus to late adverse events. Therefore, computational tools and simulations play an increasingly important role for the understanding and treatment of AD. Patient-specific digital twins have the potential to support clinical decision making and capture the complexity and interplay of the underlying physics in a tightly coupled fluid-structure interaction problem [1,2]. Unfortunately though, complex multi-physics problems still challenge modern high-performance architectures and algorithms despite the remarkable advancements made in computational hemodynamics during the past decade. Hence, aortic dissection simulations remain highly demanding, as the fluid-structure interaction problem at the very center of the disease has to be accounted for, vastly increasing computational complexity. Therefore, the number of patient-specific studies is limited and mostly based on severe simplifications regarding the constitutive modeling of tissue and blood flow. Within this contribution, we further extend a patient-specific model of a Type-B AD including flow data [3] by a multi-layered tissue model incorporating parameters of medial and adventitial layers of the aorta.

2 Methods

The subproblems of fluid-structure interaction are strongly coupled using a partitioned approach, employing the Navier-Stokes equations for incompressible flow in Arbitrary-Lagrangian Eulerian form, written in the current domain Ω_f^t as

$$\rho_f \left[\partial_t \boldsymbol{u}_f|_{\mathcal{A}_t} + \nabla \boldsymbol{u}_f \left(\boldsymbol{u}_f - \boldsymbol{u}_m\right)\right] = -\nabla p_f + \mu_f \nabla \cdot \left[\nabla \boldsymbol{u}_f + (\nabla \boldsymbol{u})^\top\right] \qquad \text{in } \Omega_f^t\,, \tag{1}$$

$$\nabla \cdot \boldsymbol{u}_f = 0 \qquad \text{in } \Omega_f^t\,, \tag{2}$$

with suitable initial and boundary conditions for a Newtonian fluid with density $\rho_f = 1060$ kg/m^3, viscosity $\mu_f = 3.5$ mPa, where $\boldsymbol{u}_m$ denotes the grid velocity and $\partial_t(\cdot)|_{\mathcal{A}_t}$ the ALE time derivative. Patient-specific volumetric flow rates as shown in Fig. 1**b** are prescribed at all in- and outlets. The initial fluid domain is reconstructed from medical image data during diastole and the fluid-structure interface is extended in outward-normal direction by 0.8 and 1.2 mm in two consecutive steps to resolve the media and adventitia layers, resulting in a computational mesh depicted in Fig. 1**a**. The balance of linear momentum including the prestress tensor $\boldsymbol{S}_0$ is formulated at time t^{n+1} in the solid reference domain $\hat{\Omega}_s$ as

$$\rho_s \ddot{\boldsymbol{d}}_s^{n+1} - \alpha \nabla \cdot \left[\boldsymbol{F}(\boldsymbol{d}_s^{n+1})\boldsymbol{S}_0 + \boldsymbol{P}(\boldsymbol{d}_s^{n+1})\right] = (1-\alpha)\nabla \cdot \left[\boldsymbol{F}(\boldsymbol{d}_s^{n})\boldsymbol{S}_0 + \boldsymbol{P}(\boldsymbol{d}_s^{n})\right] \quad \text{in } \hat{\Omega}_s\,, \tag{3}$$

with solid density $\rho_s = 1200$ kg/m^3, last timestep displacement $\boldsymbol{d}_s^n$ and deformation gradient $\boldsymbol{F} = \boldsymbol{I} + \nabla \boldsymbol{d}_s$ using HHT-α time integration and the first Piola-Kirchhoff stress tensor $\boldsymbol{P}$ defined as [4]

$$\boldsymbol{P} = \mu_s J^{-2/3}(\boldsymbol{F} - \frac{1}{3} I_1 \boldsymbol{F}^{-\top}) + \frac{\kappa_b}{2}(J^2 - 1)\boldsymbol{F}^{-\top} + \sum_{i=4,6} 2k_1 G_i \partial_{\boldsymbol{C}} G_i\,, \tag{4}$$

* Corresponding author: e-mail schussnig@tugraz.at, phone +43 316 873-6183

$$\text{with} \quad J = \det(\boldsymbol{F})\,, \quad I_1 = \operatorname{tr}(\boldsymbol{C})\,, \quad G_i = J^{-2/3}\left[\kappa_c I_1 + (1-3\kappa_c) I_i\right] - 1\,, \quad I_i = \boldsymbol{C} : \boldsymbol{A}_i$$
$$\partial_{\boldsymbol{C}} G_i = J^{-2/3}\left[\kappa_c \boldsymbol{F} + (1-3\kappa_c)\boldsymbol{F}\boldsymbol{A}_i - \frac{1}{3}\boldsymbol{F}^{-\top}\left(\kappa_c I_1 + (1-3\kappa_c) I_i\right)\right], \quad \boldsymbol{A}_i = \hat{\boldsymbol{m}}_i \otimes \hat{\boldsymbol{m}}_i\,,$$

bulk modulus $\kappa_b = 100$ kPa, fiber parameters $k_1 = 1.4$ kPa, $k_2 = 22.1$ and layer specific (flap and media/adventitia) shear modulus $\mu_s = (120/150)$ kPa and fiber dispersion $\kappa_c = (0.12/0.25)$. The prestress tensor is computed in an iterative procedure, determining a tensor field $\boldsymbol{S}_0$, which counteracts deformations due to diastolic flow in the reconstructed geometry. Mean fiber directions $\hat{\boldsymbol{m}}_i$ are constructed depending on a fiber angle $\alpha_c = \pm(27.47/52.88)^\circ$ from element-local material orientation vectors following the longitudinal and circumferential directions in the vessel wall as depicted in Fig. 1**c**. External tissue support is considered via a Robin condition (see, e.g., [3]). For further details concerning the mesh construction, prestress algorithm, material orientation and constitutive parameter choice, we refer to [5, 6].

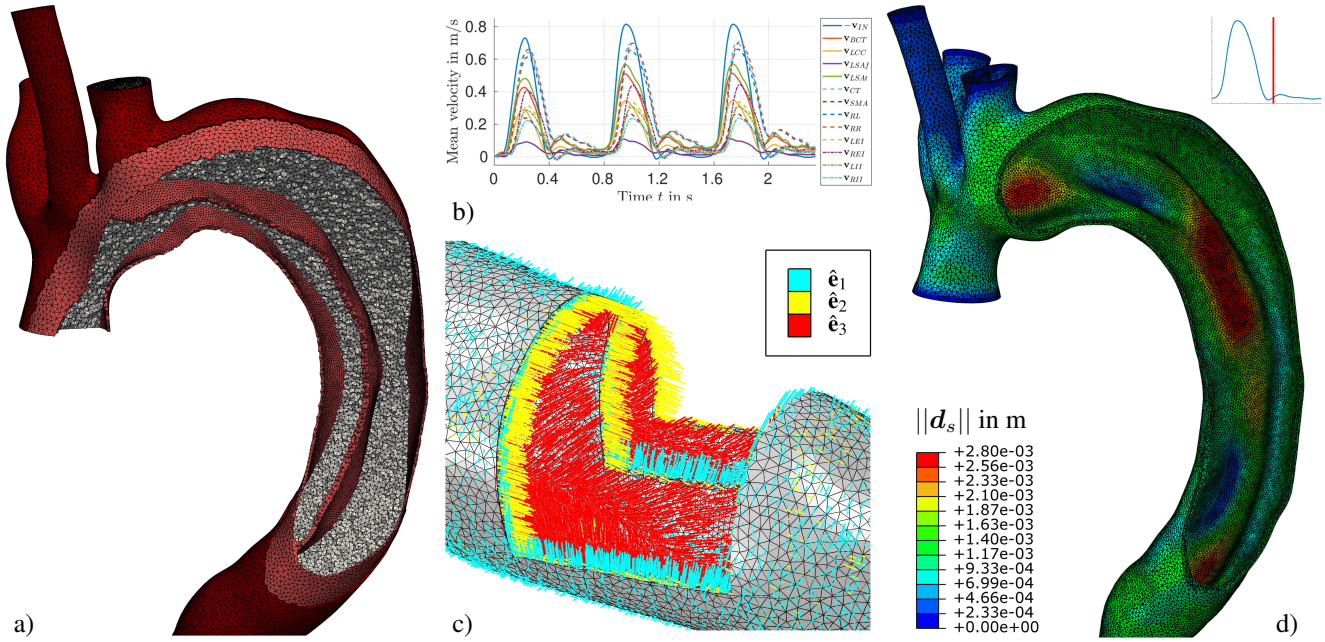

Fig. 1: a: Cut mesh in arch region resolving lumen and solid layers, **b**: patient-specific flow data from [3], **c**: close-up of material orientation vectors $\hat{\boldsymbol{e}}$ used to construct mean fiber directions $\hat{\boldsymbol{m}}_i(\alpha_c)$, and **d**: solid displacement norm $||\boldsymbol{d}_s||$ in cut arch region at $t = 2$ s.

3 Results and conclusion

Three full cardiac cycles ($T = 0.78$ s) were considered in the patient-specific simulation, resulting in a maximum displacement of ≈ 3 mm at $t = 2$ s with a complex deformation pattern in the intimal flap as seen in Fig. 1**d**. Compared to *in-vivo* measurements, displacements are underestimated in the computational model, which will be addressed in future work. Moreover, applying increasingly complex tissue models allows for a more detailed description of the vessel's response to blood flow including stresses central to the rupture process. However, difficulties connected to parameter estimation, model construction and computing times are also greatly increased. In this regard, virtual surgery and evaluation of different treatment options on digital twins remain highly demanding, motivating the further development of efficient numerical algorithms.

Acknowledgements The authors gratefully acknowledge Graz University of Technology for the financial support of the Lead-project *Mechanics, Modeling and Simulation of Aortic Dissection*.

References

[1] M. Alimohammadi, J. M. Sherwood, M. Karimpour, O. Agu, S. Balabani, and V. Díaz-Zuccarini, Biomed Eng Online **14**, 34 (2015).
[2] Y. Qiao, Y. Zeng, Y. Ding, J. Fan, K. Luo, and T. Zhu, Comput Methods Biomech Biomed Engin **22**, 620-630 (2019).
[3] K. Bäumler, V. Vedula, A. M. Sailer, J. Seo, P. Chiu, G. Mistelbauer, F. P. Chan, M. P. Fischbein, A. L. Marsden, and D. Fleischmann, Biomech Model Mechanobiol **19**, 1607-1628 (2020).
[4] T. C. Gasser, R. W. Ogden, and G. A. Holzapfel, J R Soc Interface **3**, 15-35 (2006).
[5] R. Schussnig, M. Rolf-Pissarczyk, G. A. Holzapfel, and T. P. Fries, PAMM · Proc. Appl. Math. Mech. **20**, e202000125 (2020).
[6] R. Schussnig, and T. P. Fries, 14th WCCM & ECCOMAS Congress 2020, virtual congress, doi:10.23967/wccm-eccomas.2020.109.